Bulletin of the Seismological Society of America, Vol. 109, No. 5, pp. 2125–2131, October 2019, doi: 10.1785/0120190118

Ⓔ

Short Note

Dynamic Analysis of a Large Freestanding Rock Tower (Castleton Tower, Utah)

by Jeffrey R. Moore, Paul R. Geimer, Riley Finnegan, and Clotaire Michel

Abstract We acquired a unique ambient vibration dataset from Castleton Tower, a 120 m high bedrock monolith located near Moab, Utah, to resolve dynamic and material properties of the landform. We identified the first two resonant modes at 0.8 and 1.0 Hz, which consist of mutually perpendicular, linearly polarized horizontal ground motion at the top of the tower. Damping ratios for these modes were low at ∼1%. We successfully reproduced field data in 3D numerical eigenfrequency simulation implementing a Young's modulus of 7 GPa, a value ∼30% lower than measured on core samples. Our analysis confirms that modal deformation at the first resonant frequencies closely resembles that of a cantilever beam. The outcome is that with basic estimates of geometry and material properties, the resonant frequencies of other freestanding rock monoliths can be estimated *a priori*. Such estimates are crucial to evaluate the response of rock towers to external vibration inputs.

Supplemental Content: Two animations of the modal displacement field for the first two resonant modes of Castleton Tower.

Introduction

Knowledge of the dynamic properties of slender, freestanding structures is crucial to predict their response to external forces, for example, earthquakes (Carder, 1936; Hall *et al.*, 1995; Goel and Chopra, 1997). Although more than a century of past research focused on characterizing the vibration properties of man-made civil structures (e.g., Omori, 1900; Crawford and Ward, 1964; Clinton *et al.*, 2006; Michel and Guéguen, 2010), comparably little attention has been paid to understanding the dynamics of natural structures such as rock towers (Lévy *et al.*, 2010; Bottelin *et al.*, 2013; Valentin *et al.*, 2017; Kleinbrod *et al.*, 2019). Natural rock towers are anticipated to respond in a similar dynamic manner as civil structures when excited by external forces such as wind, earthquakes, or anthropogenic energy. Therefore any effort to describe the resulting structural response, and possible damage induced by these forces, requires accurate characterization of the feature's vibrational properties. Nonetheless, field measurements of the dynamic properties of freestanding rock towers remain relatively rare (Dowding *et al.*, 1983; King, 2001; King and Demarco, 2003; Kleinbrod *et al.*, 2019).

Although methods to measure the dynamic properties of civil structures are increasingly well established (e.g., Farrar and James, 1997; Brownjohn, 2003; Michel *et al.*, 2010; Li *et al.*, 2010), measuring the dynamic properties of natural landforms presents unique challenges. Foremost is access; natural towers, for example, offer limited access to points at which vibration measurements can be made. Therefore methods to characterize the natural modes of vibration typically must rely on data stemming from only a few measurement points (as in Dowding *et al.*, 1983; King and Demarco, 2003). Furthermore for natural features of high cultural value, forced vibration modal analysis techniques are rarely permissible, so methods are restricted to those analyzing ambient vibrations (e.g., Prieto *et al.*, 2010; Moore *et al.*, 2016; Kleinbrod *et al.*, 2019). Nonetheless, experimental and analytical techniques developed for civil structures are applicable to natural landforms and can be used to generate data describing dynamic properties such as resonant frequencies, mode shapes, and damping.

In this study, we describe a rare and unique data set of ambient vibration measurements from one of the largest freestanding rock towers in the western United States, Castleton Tower located near Moab, Utah. We process a limited duration dataset of continuous ambient vibration measurements from the top of the tower to distinguish key dynamic properties for the first two resonant modes and derive an estimate for the globally averaged Young's modulus of the feature. Ultimately, our description is limited by physical access to measurement points on the tower. Nevertheless, we show that the first modes of vibration can be recreated with numerical

Downloaded from https://pubs.geoscienceworld.org/ssa/bssa/article-pdf/109/5/2125/4834142/bssa-2019118.1.pdf
by Univ Utah Marriott Library user

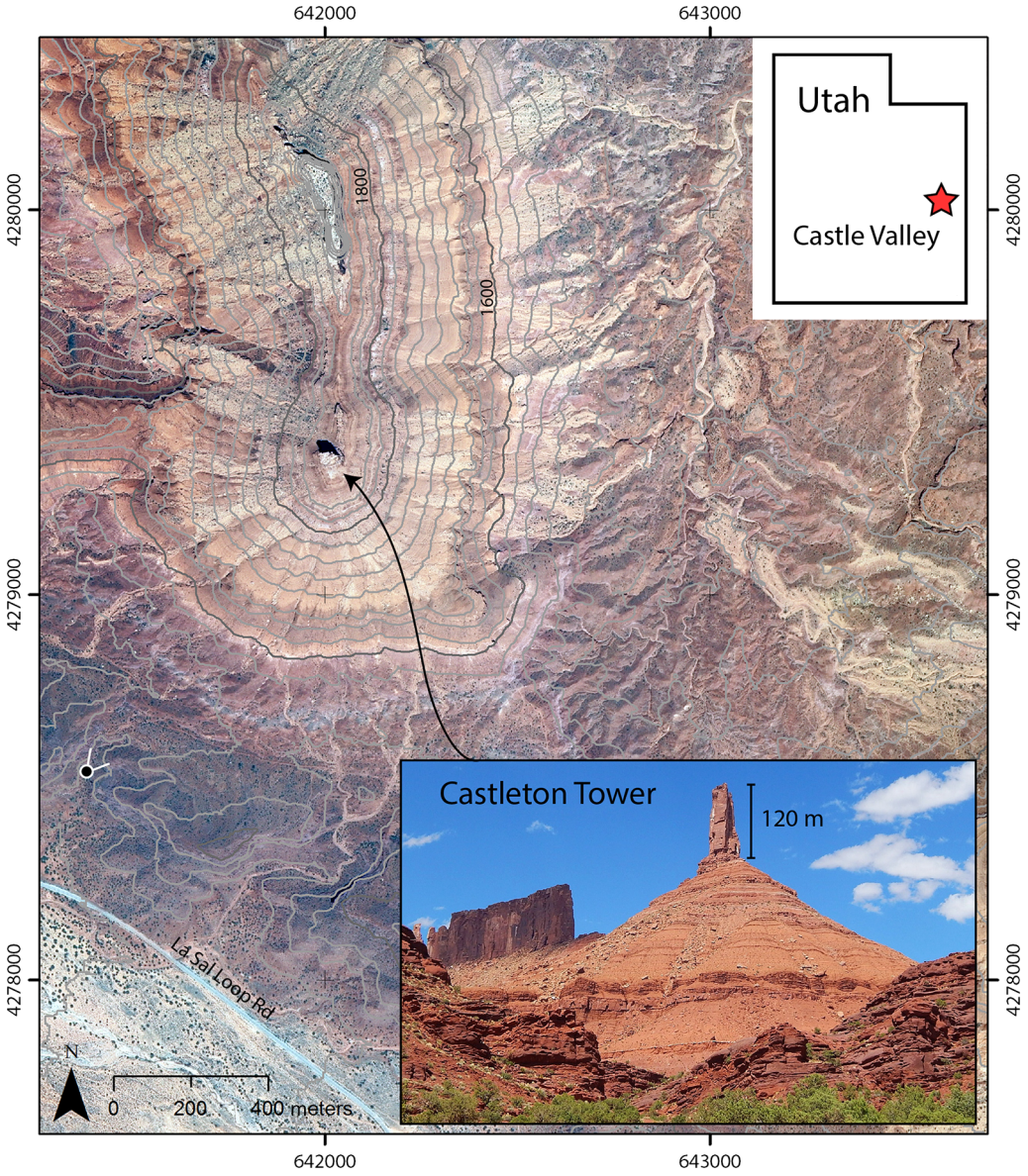

Figure 1. Map of Castleton Tower and surrounding area (see Data and Resources); contour interval is 25 m, coordinates are in meters for Universal Transverse Mercator (UTM) zone 12S. (Upper inset) Location within Utah. (Lower inset) Oblique ground-based image (credit: Ronald Scott) shows Castleton Tower—a 120 m high Wingate sandstone monolith perched atop a steep ridge composed of Chinle and Moenkopi formations (Doelling, 2002). The color version of this figure is available only in the electronic edition.

eigenfrequency simulations, and reveal valuable new information on material and dynamic properties of the tower itself. Our measurements represent a rare dataset that can be used to help predict the vibrational properties for dynamic analysis of other rock towers in Utah and worldwide.

Site Description

Castleton Tower (also known as Castle Rock) is an iconic landform of the Colorado Plateau's red-rock desert. Located 18 km northeast of Moab, Utah, the tower is a 120 m high sandstone monolith perched on the crest of a steep ridge (Fig. 1). The tower is composed of Jurassic Wingate sandstone, massive with thick beds of fine-grained, cross-bedded eolian sandstone, and red coloration reflecting high-iron content; it sits upon a steep ridge composed of Triassic Chinle and Moenkopi formations featuring alternating beds of sandstone and siltstone (Doelling, 2002). The tower's monolithic nature and solitary setting contribute to its exceptional character, drawing photographers and climbers from across the world (e.g., Roper and Steck, 1979).

Methods and Results

We conducted a field test to measure the ambient resonance of Castleton Tower on 12 March 2018 using two Nanometrics Trillium Compact three-component broadband seismometers with 24-bit Centaur data loggers. The

Downloaded from https://pubs.geoscienceworld.org/ssa/bssa/article-pdf/109/5/2125/4834142/bssa-2019118.1.pdf
by Univ Utah Marriott Library user

instruments recorded data continuously for nearly 3 hr at 100 Hz, with one seismometer located directly on top of Castleton Tower (CASTA), and the other instrument located ~100 m north of the base of the tower on the bedrock ridge serving as a reference (CASTB). Each seismometer was leveled, aligned to magnetic north, and enclosed within an insulating cover. The deploying climbers stayed with the equipment throughout the length of the recording. Because Castleton Tower is a popular climbing destination, portions of the record featured anthropogenic noise caused by climbers on the summit.

We process seismic data following methods outlined by Koper and Burlacu (2015) and Koper and Hawley (2010) to obtain frequency content and polarization attributes of ambient noise. Figure 2 compares the power spectra from stations CASTA and CASTB. We observe strong spectral peaks at 0.8 and 1.0 Hz at CASTA that are only weakly present at CASTB, which we identify as the first two resonant modes of Castleton Tower. We further obtain polarization attributes for select natural frequencies, providing azimuth and inclination of particle motion at the location of seismometer CASTA. The first two resonant frequencies of Castleton Tower show strongly polarized and mutually perpendicular, subhorizontal ground motion (Fig. 2), whereas higher order modes are observed but cannot be interpreted due to the limited spatial sampling (i.e., single sensor deployed on the tower).

We further explored the experimental dataset by processing ambient seismic recordings using the enhanced frequency domain decomposition method (see Brincker and Ventura, 2015). This method is popular in mechanical and civil engineering (e.g., Michel and Guéguen, 2018), and recently been applied to geological features such as sediment-filled valleys (Poggi *et al.*, 2015), glaciers (Preiswerk *et al.*, 2018), and rock slopes (Häusler *et al.*, 2019). The goal for the present study, which included only two sensors (six recordings), was to retrieve damping ratios. For that purpose, the selected mode bells were transformed from the frequency to the time domain, and their decay fitted by a logarithmic decrement. The first two modes were thus determined to have damping ratios of $1.1\% \pm 0.2\%$. Rare past measurements of damping ratios at other natural pinnacles have shown similarly low values (e.g., King and Demarco, 2003).

3D numerical modal analysis was used to verify our results and provide further detail of the displacement and strain fields for first resonant modes of Castleton Tower. We follow the methods of Moore *et al.* (2018) matching measured and modeled resonant frequencies, beginning with constructing a 3D photogrammetric model of the tower and its surroundings. We loaded stock aerial imagery (see Data and Resources) of the tower into ContextCapture, a photogrammetry modeling software (see Data and Resources), and combined the resulting geometry with a digital elevation model of the surrounding ridge in Meshmixer (see Data and Resources) using 5 m autocorrelated elevation data from the State of Utah (see Data and Resources). We then performed modal analysis using the finite-element software COMSOL Multiphysics (see Data and Resources), outputting eigenfrequencies and corresponding modal displacement and strain fields. In addition to geometry, COMSOL requires user-defined material properties and boundary conditions for eigenfrequency analysis. We assigned a uniform density (ρ) of 2200 kg/m^3, based on measurements from a cored block we collected in the area, and Poisson's ratio of 0.25. Because Castleton Tower is a freestanding landform, the boundary conditions were clear: we fixed the base of the model and allowed the tower and ridge to move freely. We then adjusted the Young's modulus to obtain best match between measured and modeled eigenfrequencies. Finally, we compared field measurements of polarization to displacement vectors modeled at the location of sensor CASTA.

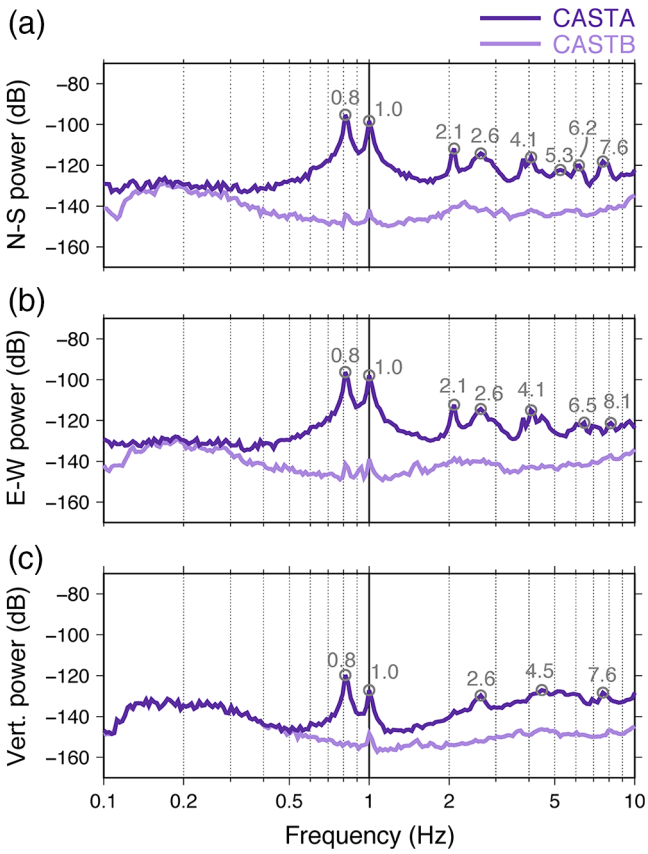

Figure 2. Power spectral density plots for station CASTA on Castleton Tower and reference station CASTB ~100 m north on the ridge for the first hour of the test (20:30–21:30 UTC). (a) North–south (N-S) horizontal, (b) east–west (E-W) horizontal, and (c) vertical (vert.) component. All hours exhibit similar spectra from which we identify the first two resonant frequencies of Castleton Tower as 0.8 and 1.0 Hz. These frequencies are labeled along with other higher spectral peaks exhibiting weaker polarization. Power is measured in decibel (dB) units of ground acceleration, $10\log_{10}(m^2/s^4/Hz)$. The color version of this figure is available only in the electronic edition.

Results of our 3D numerical modal analysis provide eigenfrequencies and the estimated globally averaged Young's modulus for Castleton Tower: the first two frequencies match the measured resonant modes of 0.8 and 1.0 Hz implementing an elastic modulus of 7.0 GPa. This corresponds to a *P*-wave velocity of ~1800 m/s and *S*-wave velocity of ~1000 m/s.

Downloaded from https://pubs.geoscienceworld.org/ssa/bssa/article-pdf/109/5/2125/4834142/bssa-2019118.1.pdf
by Univ Utah Marriott Library user

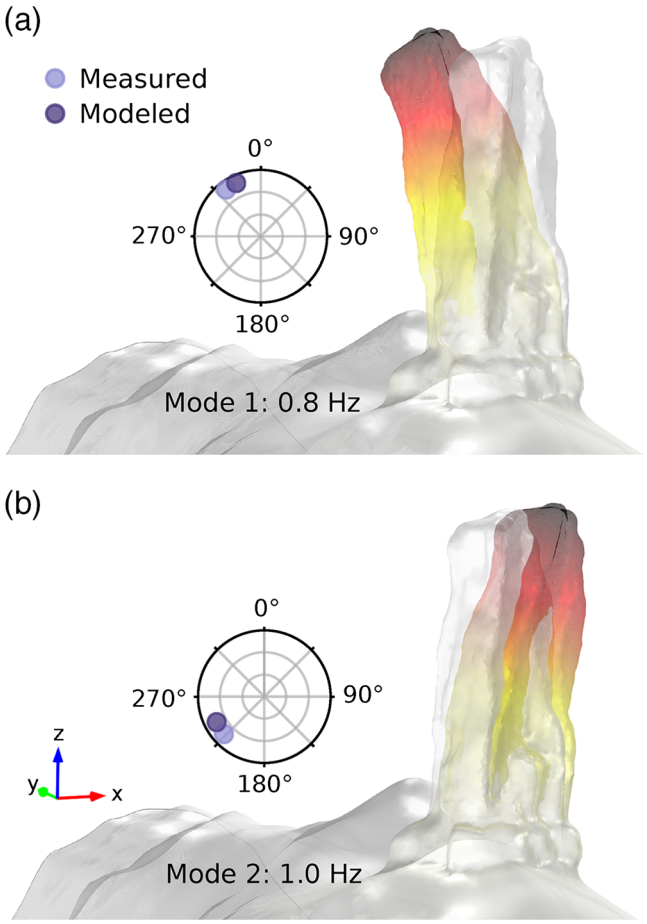

Figure 3. Modal analysis of Castleton Tower. Predicted mode shapes are shown with shading representing normalized displacement at zero phase and transparent static geometry for comparison; axis shows orientation of the model with z (vertical), y (magnetic north), and x (east). Numerical values of the measured and modeled eigenfrequencies are identical. (a) First mode = 0.8 Hz, (b) second mode = 1.0 Hz. Stereo plot insets for each compare polarization orientation for the measured motion (light circles) and modeled displacement (dark circles); radial axes are incidence at 30° increments (vertical in the center, horizontal at the perimeter), whereas polar axes show azimuth with 0°, magnetic north. The color version of this figure is available only in the electronic edition.

For comparison, we measured the Young's modulus of three Wingate sandstone cores taken from a block collected near Moab to be 9.7 ± 0.5 GPa, following suggested methods from International Society of Rock Mechanics (ISRM, 1979). The first two resonant modes represent full-height bending of the tower in mutually perpendicular directions, with peak displacement at the top of the tower and peak strain at the base of the tower. Figure 3 shows the displacement field at zero phase for the two modes, together with comparison between measured and modeled polarization vectors (animations available as Ⓔ Figs. S1 and S2 in the supplemental content to this article). Field data match numerical results closely in terms of both natural frequency and orientation of ground motion. Although we employ several simplifying assumptions in the numerical analysis, for example, uniform material properties, the excellent match between field data and numerical results indicates our model adequately represents the tower's dynamic properties for the first two resonant modes.

Discussion

Ambient vibration power spectra show two strong, distinct peaks at 0.8 and 1.0 Hz that we interpret as the first two resonant frequencies of Castleton Tower. These eigenmodes occur at relatively low frequency for natural landforms (compared to Burjánek *et al.*, 2010; Bottelin *et al.*, 2013; Valentin *et al.*, 2017; Moore *et al.*, 2018; Weber *et al.*, 2018; Kleinbrod *et al.*, 2019) and are matched by numerical eigenfrequency modeling. Simplifying assumptions used in our numerical analysis (e.g., uniform material properties and lack of fractures) are justified by the excellent match to measured frequencies and polarization vectors, and the Young's modulus derived represents a global average value for the rock mass participating in these vibrational modes, comparable to similar rock types with similar iron content (Moore *et al.*, 2018). The Young's modulus implemented in our model is lower than that measured in the laboratory because the larger rock mass of the tower incorporates macroscopic fractures and other discontinuities (e.g., bedding) not present in small core samples. Higher spectral peaks had weaker polarization and were not successfully matched in our numerical eigenfrequency simulation.

In slender structures such as rock towers or natural arches, aside from classical shear waves, the wavefield consists of dispersive (flexural) beam waves propagating in the vertical direction. These waves correspond to flexibility due to geometry of the landform. To distinguish between shear and flexural modal deformation in buildings, Boutin *et al.* (2005) and later Michel and Guéguen (2018) suggested use of the C parameter of the Timoshenko beam:

$$C = \frac{EI}{K(\frac{2L}{\pi})^2},$$

in which E is the Young's modulus, $I = \frac{bB^3}{12}$ is the moment of inertia, $K = Gk_GA$ is the shear stiffness (with A, the cross sectional area; G, the shear modulus; and k_G, the shear adjustment factor depending on the shape of the cross section of the beam), and L is the height. Assuming $L = 120$ m, $b = 50$ m, $B = 40$ m (measurements of height and width from our 3D model), and $k_G = 1$, we find $C < 0.1$ indicating the tower deforms primarily in bending.

Indeed, the modeled first two eigenmodes of Castleton Tower closely resemble the expected pattern of deformation for bending of a cantilever beam, with peak displacement at the top of the tower and peak strain at the base of the tower. Implementing the theoretical formula for the fundamental frequency of a cantilever:

$$f = \frac{1.875^2}{2\pi}\sqrt{\frac{EI}{\rho AL^4}}.$$

Downloaded from https://pubs.geoscienceworld.org/ssa/bssa/article-pdf/109/5/2125/4834142/bssa-2019118.1.pdf
by Univ Utah Marriott Library user

we reproduce the first and second measured natural frequencies assuming beam thicknesses (B) of 40 (0.8 Hz) and 50 m (1.0 Hz), respectively, with $E = 7.0$ GPa and $\rho = 2200$ kg/m^3. These thickness values approximately match the measured width of the base of Castleton Tower in directions perpendicular to each bending mode. The implication is that with basic measurements of height and thickness, the fundamental frequency of other rock towers with monolithic composition may be predicted from the theoretical formula for a cantilever. The further implication is that with the theoretical correspondence thus validated, related formulas for stress and strain could be implemented to predict the structural response of such towers under induced vibrations.

Measured vibration velocities at the resonant frequencies were up to 300 times stronger on the top of Castleton Tower (peak ground velocity = 10 μm/s) compared with the base, indicating a strongly amplified response to external excitation. Wind gusts were the primary force exciting vibration of the tower during our test. In the absence of wind-forced vibrations, however, amplification of ground motion between the top and bottom of the tower (A at a particular resonant frequency ω_k) can be estimated assuming a simple multiple-degree-of-freedom system (see the Appendix section):

$$A(\omega_k) = \frac{p_k}{2\zeta_k},$$

in which p_k is the participation factor of mode k assuming a mode shape normalized to 1 at the top, and ζ_k is its damping ratio. Beam theory indicates that p_1 lies between 1.27 (shear beam) and 1.57 (cantilever) for continuous homogeneous beams. With the observation of 1.1% damping and cantilever beam behavior, we calculate an amplification factor of ~70 at the fundamental frequency. Amplification and damping are therefore closely related.

The low-measured damping values for Castleton Tower indicate that seismic energy is trapped in the structure due to its geometry and generally unable to escape through radiation damping. The first two spectral peaks are nonetheless weakly resolved on the reference sensor CASTB (Fig. 2). Past measurements in somewhat similar settings have shown that vibrational energy from freestanding rock features can be transferred through bedrock and measured at adjacent locations. One implication of this observation is that if future resonant frequency measurements are to be made at Castleton Tower for the purpose of structural health monitoring (as in Lévy *et al.*, 2010; Starr *et al.*, 2015; Bottelin *et al.*, 2017; Burjánek *et al.*, 2018; Colombero *et al.*, 2018), climbing to the top of the tower for each new measurement may not be necessary.

We did not record any earthquakes during the short measurement interval, but with the relatively low natural frequencies around 1 Hz, Castleton Tower is expected to resonate in response to teleseisms and strong earthquakes alike, which are capable of generating energy in this frequency range (Moore *et al.*, 2016). With the strong spectral amplification anticipated, the tower will respond with ground motions far above that of surrounding bedrock, making it increasingly susceptible to earthquake-induced damage. Strong earthquakes in the region are relatively rare, however, and the seismic hazard is rated as low according to the U.S. Geological Survey (Petersen *et al.*, 2015). Assuming 5% damping, spectral acceleration for the 2500 yr return period event corresponds to about 0.5 m/s^2, which leads to a spectral displacement (peak displacement at the top of the tower) of 1.3 cm and a spectral velocity of ~8 cm/s. For 1% damping, these values increase by about 30%. Such vibration values are thought to be capable of generating rock damage (King, 2001; King and Demarco, 2003; Moore, 2018). Other sources, such as anthropogenic ground- and air-borne vibrations from transit or construction machinery, are unlikely to generate significant energy in this frequency range (Hanson *et al.*, 2006) and are therefore unlikely to excite resonance of Castleton Tower.

Conclusion

Assessing the vulnerability of freestanding rock towers to vibration inputs, including wind, earthquakes, and anthropogenic energy sources, requires knowledge of their dynamic properties. Foremost among these are natural frequencies and damping ratios, parameters that can be extracted from analysis of ambient vibration data. We analyzed one such landform, Castleton Tower, a 120 m high sandstone monolith, to provide bounds on the dynamic properties of rock towers and to assess analytical comparisons to beams. Our results revealed the first two resonant modes of vibration occur at 0.8 and 1.0 Hz and display ~1.1% damping. These low frequencies and damping ratios are caused by the large height, slenderness, and material composition of Castleton Tower. We successfully reproduced field data using 3D numerical eigenfrequency simulation, implementing a simplified uniform composition of the tower with density taken from measurements and elastic modulus determined through eigenfrequency matching. Best-matching results were achieved with a Young's modulus of 7 GPa, a value that is ~30% lower than we measured on intact core samples and that accounts for the presence of discontinuities in the tower's rock mass. Our analysis further showed that modal deformation of the tower at the first two eigenmodes closely resembles that of a cantilever beam, that is, full-height bending in mutually perpendicular directions. Observed resonant frequencies could be satisfactorily reproduced using the analytical expression for a cantilever, with material properties and geometry determined from our analysis. Our results further suggest that strong amplification of ground motion is expected at the resonant frequencies of the tower, with estimated spectral amplification between the top and base of the tower of ~70 at the fundamental mode, a result with potentially important implications for assessment of vibration-induced damage. Ultimately Castleton Tower, with its low resonant frequencies, is unlikely to be excited by low- to moderate-magnitude earthquakes with little energy in the 1 Hz range, or by anthropogenic transit and construction

Downloaded from https://pubs.geoscienceworld.org/ssa/bssa/article-pdf/109/5/2125/4834142/bssa-2019118.1.pdf
by Univ Utah Marriott Library user

sources. Our methodology can be easily implemented at other rock towers to predict dynamic properties in support of vibration vulnerability assessment.

Data and Resources

Data generated and analyzed in this study are available for download from the website https://geohazards.earth.utah.edu/data.html (last accessed March 2019). Additional data used in this article came from published sources listed in the references. Stock aerial imagery is available at axiomimages.com (last accessed March 2019). ContextCapture, a photogrammetry modeling software, is available at bentley.com (last accessed April 2018). Meshmixer is available at meshmixer.com (last accessed June 2018). Utah Automated Geographic Reference Center (AGRC) is available at gis.utah.gov (last accessed March 2019). COSMOL Multiphysics software is available at comsol.com (last accessed May 2018).

Acknowledgments

Kathryn Vollinger and Natan Richman skillfully ascended Castleton Tower generating the data that made this analysis possible. The authors are grateful to Michael Thorne and Keith Koper for help processing seismic data. Comments from Rasool Anooshehpoor and an anonymous reviewer helped improve this article. This work was funded by the National Science Foundation Grant Number EAR-1831283.

References

Bottelin, P., L. Baillet, E. Larose, D. Jongmans, D. Hantz, O. Brenguier, H. Cadet, and A. Helmstetter (2017). Monitoring rock reinforcement works with ambient vibrations: La Bourne case study (Vercors, France), *Eng. Geol.* **226,** 136–145.

Bottelin, P., C. Levy, L. Baillet, D. Jongmans, and P. Gueguen (2013). Modal and thermal analysis of Les Arches unstable rock column (Vercors massif, French Alps), *Geophys. J. Int.* **194,** 849–858.

Boutin, C., S. Hans, E. Ibraim, and P. Roussillon (2005). In situ experiments and seismic analysis of existing buildings. Part II: Seismic integrity threshold, *Earthq. Eng. Struct. Dynam.* **34,** 1531–1546.

Brincker, R., and C. Ventura (2015). *Introduction to Operational Modal Analysis*, Wiley, Hoboken, New Jersey.

Brownjohn, J. M. (2003). Ambient vibration studies for system identification of tall buildings, *Earthq. Eng. Struct. Dynam.* **32,** 71–95.

Burjánek, J., V. Gischig, J. R. Moore, and D. Fäh (2018). Ambient vibration characterization and monitoring of a rock slope close to collapse, *Geophys. J. Int.* **212,** 297–310.

Burjánek, J., G. Stamm, V. Poggi, J. R. Moore, and D. Fäh (2010). Ambient vibration analysis of an unstable mountain slope, *Geophys. J. Int.* **180,** 820–828.

Carder, D. S. (1936). Observed vibrations of buildings, *Bull. Seismol. Soc. Am.* **26,** 245–277.

Clinton, J. F., S. Case Bradford, T. H. Heaton, and J. Favela (2006). The observed wander of the natural frequencies in a structure, *Bull. Seismol. Soc. Am.* **96,** 237–257.

Colombero, C., L. Baillet, C. Comina, D. Jongmans, E. Larose, J. Valentin, and S. Vinciguerra (2018). Integration of ambient seismic noise monitoring, displacement and meteorological measurements to infer the temperature-controlled long-term evolution of a complex prone-to-fall cliff, *Geophys. J. Int.* **213,** 1876–1897.

Crawford, R., and H. S. Ward (1964). Determination of the natural periods of buildings, *Bull. Seismol. Soc. Am.* **54,** 1743–1756.

Doelling, H. H. (2002). Geologic map of the Fisher Towers 7.5' Quadrangle, Grand County, Utah, *Utah Geol. Surv. Map 183*, 22 pp.

Dowding, C. H., F. S. Kendorski, and R. A. Cummings (1983). Response of rock pinnacles to blasting vibrations and airblasts, *Environ. Eng. Geosci.* **20,** 271–281.

Farrar, C. R., and G. H. James III (1997). System identification from ambient vibration measurements on a bridge, *J. Sound Vib.* **205,** 1–18.

Goel, R. K., and A. K. Chopra (1997). Period formulas for moment-resisting frame buildings, *J. Struct. Eng.* **123,** 1454–1461.

Hall, J. F., T. H. Heaton, M. W. Halling, and D. J. Wald (1995). Near-source ground motion and its effects on flexible buildings, *Earthq. Spectra* **11,** 569–605.

Hanson, C. E., D. A. Towers, and L. D. Meister (2006). Transit noise and vibration impact assessment, *U.S. Dept. Transport. Federal Trans. Admin. Rept. FTA-VA-90-1003-06*, 274 pp.

Häusler, M., C. Michel, J. Burjánek, and D. Fäh (2019). Fracture network imaging on rock slope instabilities using resonance mode analysis, *Geophys. Res. Lett* **46,** no. 12, 6497–6506, doi: 10.1029/2019GL083201.

International Society of Rock Mechanics (ISRM) (1979). Suggested methods for determining the uniaxial compressive strength and deformability of rock materials, *Int. J. Rock Mech. Min. Sci. Geomech. Abstr.* **16,** 135–140.

King, K. W. (2001). Chiricahua pinnacle vibration investigation, *National Park Service Preliminary Rept.*, 39 pp.

King, K. W., and M. J. DeMarco (2003). Impacts of construction vibrations on rock pinnacles and natural bridges, General Hitchcock Highway, Tucson, AZ, *Proc. Third International Conference on Applied Geophysics*, Orlando, Florida, 8–12 December.

Kleinbrod, U., J. Burjánek, and D. Fäh (2019). Ambient vibration classification of unstable rock slopes: A systematic approach, *Eng. Geol.* **249,** 198–217.

Koper, K. D., and R. Burlacu (2015). The fine structure of double-frequency microseisms recorded by seismometers in North America, *J. Geophys. Res.* **120,** 1677–1691.

Koper, K. D., and V. L. Hawley (2010). Frequency dependent polarization analysis of ambient seismic noise recorded at a broadband seismometer in the central United States, *Earthq. Sci.* **23,** 439–447.

Lévy, C., L. Baillet, D. Jongmans, P. Mourot, and D. Hantz (2010). Dynamic response of the Chamousset rock column (Western Alps, France), *J. Geophys. Res.* **115,** doi: 10.1029/2009JF001606.

Li, Q. S., L. H. Zhi, A. Y. Tuan, C. S. Kao, S. C. Su, and C. F. Wu (2010). Dynamic behavior of Taipei 101 tower: Field measurement and numerical analysis, *J. Struct. Eng.* **137,** 143–155.

Michel, C., and P. Guéguen (2010). Time-frequency analysis of small frequency variations in civil engineering structures under weak and strong motions using a reassignment method, *Struct. Heal. Monit.* **9,** 159–171, doi: 10.1177/1475921709352146.

Michel, C., and P. Guéguen (2018). Interpretation of the velocity measured in buildings by seismic interferometry based on Timoshenko beam theory under weak and moderate motion, *Soil Dynam. Earthq. Eng.* **104,** 131–142.

Michel, C., P. Guéguen, S. El Arem, J. Mazars, and P. Kotronis (2010). Full-scale dynamic response of an RC building under weak seismic motions using earthquake recordings, ambient vibrations and modelling, *Earthq. Eng. Struct. Dynam.* **39,** 419–441.

Moore, J. R. (2018). Rainbow Bridge vibration risk assessment: Ambient vibration testing and computer modeling results for Rainbow Bridge, *Natural Res. Rept. NPS/RABR/NRR—2018/1617*, National Park Service, Fort Collins, Colorado, 70 pp.

Moore, J. R., P. R. Geimer, R. Finnegan, and M. Thorne (2018). Use of seismic resonance measurements to determine the elastic modulus of freestanding rock masses, *Rock Mech. Rock Eng.* **51,** 3937–3944.

Moore, J. R., M. S. Thorne, K. D. Koper, J. R. Wood, K. Goddard, R. Burlacu, S. Doyle, E. Stanfield, and B. White (2016). Anthropogenic sources stimulate resonance of a natural rock bridge, *Geophys. Res. Lett.* **43,** 9669–9676.

Downloaded from https://pubs.geoscienceworld.org/ssa/bssa/article-pdf/109/5/2125/4834142/bssa-2019118.1.pdf
by Univ Utah Marriott Library user

Omori, F. (1900). Earthquake measurement in a brick building, *Publ. Earthq. Investig. Comm. Foreign Lang.* **4,** 7–11.

Petersen, M. D., M. P. Moschetti, P. M. Powers, C. S. Mueller, K. M. Haller, A. D. Frankel, Y. Zeng, S. Rezaeian, S. C. Harmsen, O. S. Boyd, and N. Field (2015). The 2014 United States national seismic hazard model, *Earthq. Spectra* **31,** S1–S30.

Poggi, V., L. Ermert, C. Michel, and D. Fäh (2015). Modal analysis of 2-D sedimentary basin from frequency domain decomposition of ambient vibration array recordings, *Geophys. J. Int.* **200,** 615–626.

Preiswerk, L. E., C. Michel, F. Walter, and D. Fäh (2018). Effects of geometry on the seismic wavefield of Alpine glaciers, *Ann. Glaciol.* 1–13, doi: 10.1017/aog.2018.27.

Prieto, G. A., J. F. Lawrence, A. I. Chung, and M. D. Kohler (2010). Impulse response of civil structures from ambient noise analysis, *Bull. Seismol. Soc. Am.* **100,** 2322–2328.

Roper, S., and A. Steck (1979). *Fifty Classic Climbs in North America*, Sierra Club Books, San Francisco, California, 324 pp.

Starr, A. M., J. R. Moore, and M. S. Thorne (2015). Ambient resonance of Mesa Arch, Canyonlands National Park, Utah, *Geophys. Res. Lett.* **42,** 6696–6702.

Valentin, J., A. Capron, D. Jongmans, L. Baillet, P. Bottelin, F. Donze, E. Larose, and A. Mangeney (2017). The dynamic response of prone-to-fall columns to ambient vibrations: Comparison between measurements and numerical modelling, *Geophys. J. Int.* **208,** 1058–1076, doi: 10.1093/gji/ggw440.

Weber, S., D. Fäh, J. Beutel, J. Faillettaz, S. Gruber, and A. Vieli (2018). Ambient seismic vibrations in steep bedrock permafrost used to infer variations of ice-fill in fractures, *Earth Planet. Sci. Lett.* **501,** 119–127.

Appendix

Amplification of Seismic Motion at the Resonant Frequencies of a Multiple Degree-of-Freedom System

The response of the kth single-degree-of-freedom (SDOF) system in the Fourier domain is written as:

$$\hat{S}_k(\omega) = \frac{\omega_k^{'}}{\omega_k^{'2} + (\zeta_k \omega_k + i\omega)^2},$$

in which ω_k is the angular resonance frequency, ζ_k is the viscous damping ratio, and $\omega_k^{'2} = \omega_k^2(1 - \zeta_k^2)$.

In the Fourier domain, the total displacement $\hat{U}_t(\omega)$ of the multiple degree-of-freedom system (with N degree of freedom) at point 1 (top of the structure) resulting from the ground acceleration $\hat{U}_g^{''}(\omega)$ is computed by modal summation of the response of each SDOF system (Duhamel integral, see for instance Goel and Chopra, 1997):

$$\begin{aligned}\hat{U}_t(\omega) &= \sum_{k=1}^{N} \phi_{1k} \frac{-p_k}{\omega_k^{'}} (\hat{U}_g^{''}(\omega) \times \hat{S}_k(\omega)) + \hat{U}_g(\omega) \\ &= \hat{U}_g(\omega)\left(\sum_{k=1}^{N} \frac{\phi_{1k} p_k \omega^2}{\omega_k^{'2} + (\zeta_k \omega_k + i\omega)^2} + 1\right) \\ &= \hat{U}_g(\omega)\left(\sum_{k=1}^{N} \frac{\phi_{1k} p_k}{(\frac{\omega_k}{\omega})^2 + 2i\zeta_k \frac{\omega_k}{\omega} - 1} + 1\right).\end{aligned}$$

With ϕ_{1k} being the modal shape at point 1 (top of the structure) and p_k is the participation factor of mode k. As a reminder, p_k is defined as:

$$p_k = \frac{\phi_k^T \mathbf{M} \Delta}{\phi_k^T \mathbf{M} \phi_k},$$

in which $\mathbf{M}$ is the mass matrix and Δ is a vector of ones. p_k depends on normalization of the mode shape ϕ_k.

Therefore, the amplification factor A in the Fourier domain is

$$A(\omega) = \left|\frac{\hat{U}_t(\omega)}{\hat{U}_g(\omega)}\right| = \left|\sum_{k=1}^{N} \frac{\phi_{1k} p_k}{(\frac{\omega_k}{\omega})^2 + 2i\zeta_k \frac{\omega_k}{\omega} - 1} + 1\right|.$$

This corresponds to a high-pass filter of second order. At $\omega = \omega_k$, assuming that only mode k has energy and considering p_k corresponding to a mode shape normalized at the top ($\phi_{1k} = 1$), the amplification can be written as

$$A(\omega_k) = \left|\frac{p_k}{1 + 2i\zeta_k - 1} + 1\right| = \sqrt{\left(\frac{p_k}{2\zeta_k}\right)^2 + 1} \approx \frac{p_k}{2\zeta_k}.$$

Amplification and damping ratio are thus closely related, simply modulated by a geometric factor expressing the participation of the mode.

Jeffrey R. Moore
Paul R. Geimer
Riley Finnegan
Department of Geology and Geophysics
University of Utah
Sutton Building
115 S 1460 E, Room 383
Salt Lake City, Utah 84112-0102 U.S.A.
jeff.moore@utah.edu

Clotaire Michel
Swiss Seismological Service
Swiss Federal Institute of Technology of Zürich
Sonneggstrasse 5
CH-8092 Zürich, Switzerland

Manuscript received 14 May 2019;
Published Online 27 August 2019

Downloaded from https://pubs.geoscienceworld.org/ssa/bssa/article-pdf/109/5/2125/4834142/bssa-2019118.1.pdf
by Univ Utah Marriott Library user